Supplementary information for "Ash Fingers Modify Tephra Sedimentation During a Coarse-Ash-Dominated Eruption: Evidence from the 23 July 2024 Etna Paroxysm"

Carolina Díaz-Vecino[1], Jonathan Lemus[1,2], Allan Fries[1], Riccardo Simionato[1,2], Simon Thivet[1,3], Simona Scollo[4], Francesco Amadio[5], Laura Pioli[5], Alexandros Panagiotis Poulidis[6], Valentin Freret-Lorgeril[7] and Costanza Bonadonna[1]

[1] Department of Earth Sciences, University of Geneva, Geneva, 1205, Switzerland.
[2] Department of Computer Science, University of Geneva, Carouge, 1227, Switzerland
[3] Department of Geosciences, University of Fribourg, Fribourg, 1700, Switzerland
[4] Istituto Nazionale di Geofisica e Vulcanologia, Osservatorio Etneo, Piazza Roma 2, 95125 Catania, Italy.
[5] Dipartimento di Scienze Chimiche e Geologiche, Università di Cagliari, Cittadella Universitaria, Monserrato 09042, Italy.
[6] Institute of Environmental Physics, University of Bremen, 28359, Bremen, Germany
[7] Laboratoire Magmas Et Volcans, Université Clermont Auvergne, CNRS, 63000 Clermont-Ferrand, IRD, OPGC, France

Correspondence to: Carolina Diaz-Vecino (carolinadiazvecino@gmail.com)

1. Geometrical calibration

This section provides a visual representation of the workflow used to extract the geometrical parameters required for the image calibration required as input into the PlumeTraP program (Simionato et al., 2022), illustrating how image-based measurements are translated into input parameters.

Using the minimum camera-image plane distance γ^{near}, maximum camera-image plane distance γ^{far}, horizontal Field Of View (FOV) θ_h, vertical FOV θ_v, and inclination of the camera ϕ. The values of θ_h, γ^{far} and θ_v were derived from Google Earth, as illustrated in **Supplementary Figure S1A**. The vertical field of view was then obtained from the horizontal field of view using:

$$\theta_v = \theta_h \frac{N_i}{M_i}, \qquad \textbf{Eq. S1}$$

where N_i and M_i are the image height and width in pixels, respectively. The camera inclination was determined following the methodology of Snee et al., (2023):

$$\phi = tan^{-1}\left(\frac{z_{ref} - z_{cam}}{d\prime}\right) + tan^{-1}\left[\left(1 - \frac{2j_{ref}}{N_i}\right) tan\left(\frac{\theta_v}{2}\right)\right], \qquad \textbf{Eq. S2}$$

where d' is the horizontal distance between the camera and the reference point in the image frame (approximately the mean of γ^{near} and γ^{far}); z_{cam} is the camera altitude derived from Google Earth; z_{ref} is the reference height, taken as the vent elevation; and j_{ref} is the pixel coordinate of the reference point **Supplementary Figure S1B.** All calibration parameters are reported in **Table S1.**

Table S1 Geometrical parameters used as input in PlumeTraP for the three calibrations used in the present analysis. It includes the time interval for each calibration.

Calibration	Time (LT)	γ^{near} (km)	γ^{far} (km)	d' (km)	θ_h	θ_v	M_i	N_i	z_{ref}
Cal-1	06:39 - 08:24	15.93	16.57	16.25	51.12	28.75	1920	1080	3.3
Cal-2	08:24 – 09:13	16.35	16.49	16.25	34.00	19.12	1920	1080	3.3
Cal-3	09:13 - 10:00	15.31	16.63	16.25	55.90	31.44	1920	1080	3.3

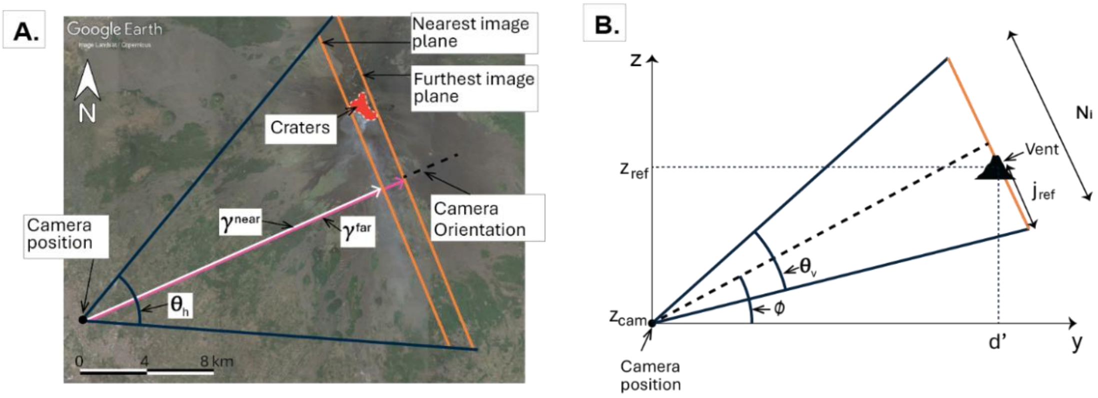

Figure S1 Geometrical calibration used for plume tracking **(A)** Google Earth image of Etna illustrating the configuration involved in the calibration methodology of Simionato et al., (2022) to determine key geometrical parameters required as input for the PlumeTraP software, including the minimum and maximum camera-image plane distances (γ^{near}, γ^{far}) and the horizontal field of view (θ_h). **(B)** Schematic side view of the calibration approach illustrating the vertical field of view (θ_v), the camera inclination (ϕ), and reference geometry (z_{ref}, z_{cam}, j_{ref} and d'). Sketch modified from Snee et al., (2023)

2. Disdrometer velocity calculations

To ensure the reliability of the disdrometer measurements, raw particle detections were filtered to remove physically implausible signals. The filtering procedure follows the approach of Freret-Lorgeril et al. (2022) and is based on theoretical settling-velocity constraints.

First, margin fallers were identified and removed. These correspond to small particles (< 0.3 mm) exhibiting anomalously high settling velocities, typically generated when particles partially intersect the laser beam near its edges, leading to an underestimation of particle size. Second, particles with unrealistically low settling velocities for their size were excluded. These detections fall below the minimum physically expected velocity derived from theoretical settling relationships and are therefore inconsistent with gravitational settling behavior. As illustrated in **Figure S2**, the application of these filters isolates a subset of particles that follow physically consistent size–velocity trends, forming the basis for all subsequent analyses.

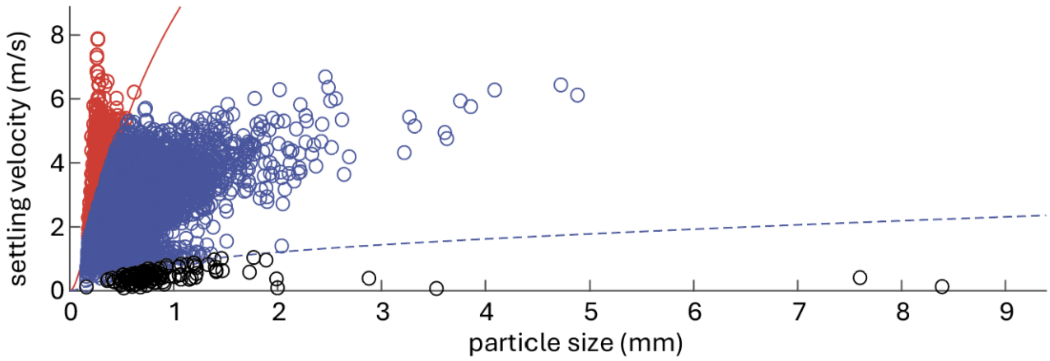

Figure S2. Particle size versus settling velocity measured with the disdrometers at L1 location. Blue circles represent the clean-filtered dataset, bounded by the red and blue curves used as filtering thresholds. Red circles indicate margin fallers (particles detected at the edge of the sampling area), while black circles correspond to particles that have lower velocities than physically expected.

3. Total Erupted Mass (TEM) calculations

Table S2. TEM estimates for the July 23, 2024 Mount Etna volcano eruption obtained using four different fitting methods: straight-line exponential (Pyle, 1989), two-segment straight-line exponential (Fierstein and Nathenson, 1992), power-law (Bonadonna and Houghton, 2005), and Weibull (Bonadonna and Costa, 2012) approaches. Values were derived from the integration of the measured tephra mass-loading dataset.

Fitting method	**TEM (kg)**
Straight-line exponential	1.33×10^8
Two segments straight-line exponential	1.14×10^8
Power Law	$1.07E \times 10^8$
Weibull	$1.25E \times 10^8$

4. Density calculations using water pycnometry

Table S3. Particle density measurements obtained from water pycnometry for selected grain size fractions from samples collected at location L1.

Sample #	**Size (μm)**	**Calculated Density**	**Uncertainty on the density**

		(kg m^{-3})	(kg m^{-3})
B2	500	2528.95	12.49
B2	500	2849.74	1.39
B1	710	2225.94	22.97
B1	710	2122.02	26.57
B1	1000	1472.77	49.03
T3	1000	1766.54	38.87

5. Tephra 2 code modification and initial parameters

```
double part_fall_time(double particle_ht, double layer, double
   ashdiam, double part_density) {

  double rho, hz, temp0, temp1;
  double vtl, vti, vtt;
  double reynolds_number;
  double particle_term_vel;
  double particle_fall_time;

  particle_fall_time = 0.0;
  hz = particle_ht; /* height of the particle above sea level */

  /*rho is the density of air (kg/m^3) at the elevation of the
     current
   * particle*/
  temp0 = -hz / 8200.0;
  rho = AIR_DENSITY * exp(temp0);

  /*
  (friction due to the air) :
  vtl is terminal velocity (m/s) in laminar regime RE<6
  vti is terminal velocity (m/s) in intermediate regime 6<RE<500
  vtt is terminal velocity (m/s) in turbulent regime RE>500
  */
  vtl = part_density * GRAVITY * ashdiam * ashdiam /
        AIR_VISCOSITY_x_18; /* 18.0 * AIR_VISCOSITY */

  /*
  vti = ashdiam *
  pow(((4.0*GRAVITY*GRAVITY*erupt->part_mean_density *erupt->
     part_mean_density
  )/        (225.0*AIR_VISCOSITY*rho)),(1.0/3.0));
  vtt=sqrt(3.1*erupt->part_mean_density *GRAVITY*ashdiam/rho);
  */

  /*
  RE is calculated using vtl (RE is Reynolds Number)
  */
  reynolds_number = ashdiam * rho * vtl / AIR_VISCOSITY;
  particle_term_vel = vtl;
  temp0 = ashdiam * rho;

  /*
  c...if laminar RE>6 (intermediate regime), RE is calculated again
     considering
  vti
```

Continue →

```c
if (reynolds_number >= 6.0) {

  /*4.0 * GRAVITY * GRAVITY * part_density * part_density / AIR_VISCOSITY *
   * 225.0 * rho */
  /*temp1 = GRAV_SQRD_x_4 * part_density * part_density / AIR_VISCOSITY_x_225
   * * rho; */
  /*Added parentheses around deniminator - 04/23/2012 */
  temp1 = GRAV_SQRD_x_4 * part_density * part_density /
          (AIR_VISCOSITY_x_225 * rho);
  vti = ashdiam * pow(temp1, ONE_THIRD); /* ONE_THIRD = 1.0/3.0 */
  reynolds_number = temp0 * vti / AIR_VISCOSITY;
  particle_term_vel = vti;
  /*
  c...if intermediate RE>500 (turbulent regime), RE is calculated again
  considering vtt
  */
  if (reynolds_number >= 500.0) {
    vtt = sqrt(3.1 * part_density * GRAVITY * ashdiam / rho);
    reynolds_number = temp0 * vtt / AIR_VISCOSITY;
    particle_term_vel = vtt;
  }
}
```

```c
if (SDGIS == 1 && ashdiam < DIAM_C) {
  particle_term_vel = VF;
}
```

```c
/* Calculate the time it takes this particle to fall through this
 * distance=layer */
particle_fall_time = layer / particle_term_vel;

/* particle fall time is in sec   */

// printf("i= %d, layer = %f, hz = %f, particle_term_vel = %f, diam=%f,
// reynolds = %f\n", i,layer_thickness, hz, particle_term_vel, a//shdiam,
// reynolds_number);

return particle_fall_time;
}
```

Figure S3. Excerpt from the **part_fall_time** function in the **/common_src/tephra2_calc.c** source file showing the implementation of ash-finger settling in TEPHRA2. The highlighted section (red box) contains the only modification introduced to the original code: whenever a particle size class is smaller than the critical diameter (d_{max}), its individual terminal settling velocity is replaced by the measured ash-finger descent velocity (V_f). The resulting settling velocity is subsequently used to calculate the particle fall time from the particle release height.

Table S3. Input parameters used in the Tephra2 simulations for the 23 July 2024, Etna eruption. The table includes eruption source parameters, vent location and elevation, grain-size range, particle densities, column discretization settings, and diffusion-related parameters used to simulate tephra transport and sedimentation. Both the standard and modified ash finger simulations were initialized using the same input parameters.

Input	Value
Plume height (m)	9233
Eruption mass (kg m^{-2})	1.20×10^8
Vent easting	500024.03
Vent northing	4177699.5
Vent elevation	3357
Max grain size (ϕ)	-6
Min grain size (ϕ)	8
Eddy const	4.00×10^{-2}
Lithic density (kg m^{-3})	2700
Pumice density (kg m^{-3})	1024
Col steps	100
Part steps	100
Plume model	2
Alpha	3
Beta	1.4
Fall time threshold (s)	200000
Diffusion coefficient (m^2 s^{-1})	130

6. Estimation of wind-driven organization timescales for ash finger formation

To assess whether ambient wind may have contributed to the spatial organization of ash fingers during the 23 July 2024, eruption of Etna volcano, we applied the conceptual framework proposed by Freret-Lorgeril et al., (2020). In this framework, wind shear induces counter-rotating rolls within the drifting ash cloud, locally enhancing particle concentration at the cloud base and promoting settling-driven gravitational instabilities.

The characteristics timescale for wind-driven organization of the plume is defined as:

$$t_w = \frac{h}{v_w}, \quad \textbf{Eq. S3}$$

Where h is the characteristic plume width and v_w is the ambient wind speed at the altitude of finger formation. The parameter h was estimated directly from the visible-wavelength image acquired during the finger-forming phase of the eruption (**Figure S4**), yielding $h \approx 1385$ m. Wind velocities were derived from WRF atmospheric profiles constrained to the altitude interval between the minimum and maximum plume height observed and the time when ash fingers were observed beneath the cloud. Because wind speed varied with altitude during the time interval, giving a representative value of v_w = 16 ± 5 m s^{-1} was adopted.

Using these values, the wind-organization timescale is:

$$t_w = \frac{1385}{16} \approx 86\text{s} \,, \qquad \textbf{Eq. S4}$$

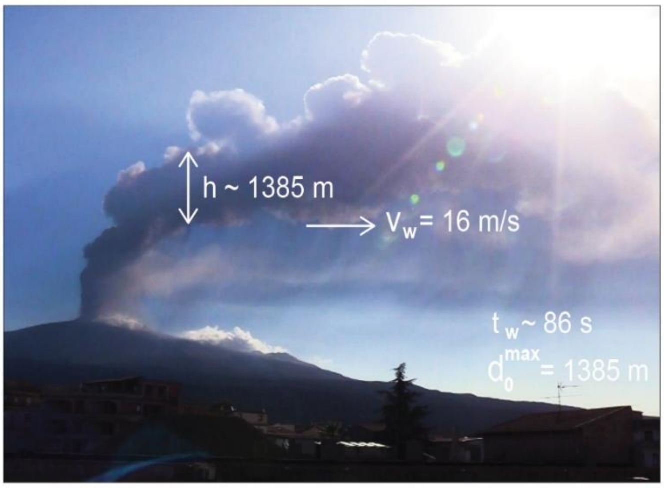

Figure S4. Visible-wavelength image of the July 23, 2024 paroxysmal eruption of Etna at t= 08:24 LT (UTC +2) illustrating the scaling analysis used to assess the potential influence of wind-driven organization on ash finger formation, following the conceptual framework of Freret-Lorgeril et al., (2020)

References

Bonadonna, C., Costa, A., 2012. Estimating the volume of tephra deposits: A new simple strategy. Geology 40, 415–418. https://doi.org/10.1130/G32769.1

Bonadonna, C., Houghton, B.F., 2005. Total grain-size distribution and volume of tephra-fall deposits. Bull Volcanol 67, 441–456. https://doi.org/10.1007/s00445-004-0386-2

Fierstein, J., Nathenson, M., 1992. Another look at the calculation of fallout tephra volumes. Bull Volcanol 54, 156–167. https://doi.org/10.1007/BF00278005

Freret-Lorgeril, V., Gilchrist, J., Donnadieu, F., Jellinek, A.M., Delanoë, J., Latchimy, T., Vinson, J.P., Caudoux, C., Peyrin, F., Hervier, C., Valade, S., 2020. Ash sedimentation by fingering and sediment thermals from wind-affected volcanic plumes. Earth and Planetary Science Letters 534, 116072. https://doi.org/10.1016/j.epsl.2020.116072

Pyle, D.M., 1989. The thickness, volume and grainsize of tephra fall deposits. Bull Volcanol 51, 1–15. https://doi.org/10.1007/BF01086757

Simionato, R., Jarvis, P.A., Rossi, E., Bonadonna, C., 2022. PlumeTraP: A New MATLAB-Based Algorithm to Detect and Parametrize Volcanic Plumes from Visible-Wavelength Images. Remote Sensing 14, 1766. https://doi.org/10.3390/rs14071766

Snee, E., Jarvis, P.A., Simionato, R., Scollo, S., Prestifilippo, M., Degruyter, W., Bonadonna, C., 2023. Image analysis of volcanic plumes: A simple calibration tool to correct for the effect of wind. Volcanica 6, 447–458. https://doi.org/10.30909/vol.06.02.447458